A phase-transfer-assisted synthesis of cysteine-Ag nanoparticles/graphene oxide nanocomposite and its enhanced performance in antibiosis and biosensing

To cite this article before publication: Zhizhan Wang *et al* 2020 *Nanotechnology* in press https://doi.org/10.1088/1361-6528/aba05c

IOP Publishing Journal Title
Journal **XX** (XXXX) XXXXXX https://doi.org/XXXX/XXXX

A phase-transfer-assisted synthesis of cysteine-Ag nanoparticles/graphene oxide nanocomposite and its enhanced performance in antibiosis and biosensing

ZhiZhan Wang[1], Fei Li[2,*], Li Zhang[1,*], JunZhi Qian[1], Shaokui Cao[1,*]

[1] School of Materials Science and Engineering, Zhengzhou University, Zhengzhou, China
[2] School of Intelligent Engineering, Jiangxi University of Technology, Nanchang, China

E-mail: tianxianghunter@126.com (Fei Li), lizhang9@zzu.edu.cn (Li Zhang), caoshaokui@zzu.edu.cn (Shaokui Cao)

Received xxxxxx
Accepted for publication xxxxxx
Published xxxxxx

Abstract

We report a facile, rapid, phase-transfer-assisted process to prepare Ag nanoparticles (AgNP) loaded graphene oxide (GO) nanocomposite, by using cysteine as a high-effective phase transfer agent for AgNP movement from organic phase to water and subsequently as a covalent linkage for immobilizing AgNP on GO. The obtained *c*-Ag/GO nanocomposite possesses high nanoparticle loading efficiency, small particle size and monodispersity, strong binding force, and good water dispersibility, which endow it a great potential in a variety of bio-applications. As the illustrations of application, *c*-Ag/GO and its derivatives *c*-Ag/rGO were used for antibiosis and biosensing respectively. The *c*-Ag/GO composite shows the high antibacterial activity against *E. coli* with a minimal bactericidal concentration of 10 μg/mL. And the biosensor based on *c*-Ag/rGO exhibits the rapid and sensitive response for uric acid detection with a detection limit of 0.025 μM, a sensitivity of 5.76 μA/mM, and wide linear range of 0.025~2250 μM. The comparative analysis with relevant nanocomposites also reveals the precedence of *c*-Ag/GO in these applications, thus highlighting the advantages of the developed preparation method for *c*-Ag/GO.

Keywords: phase transfer, silver nanoparticle, graphene oxide, antibacterial, biosensor

1. Introduction

Silver nanoparticles (AgNP) have drawn considerable attention in the fields of optoelectronics, antibiosis, catalysis and sensor, owing to their unique chemical and physical properties.[1, 2] The performances of AgNP depend heavily on their shape, particle size and dispersity, which are determined by the specific synthetic methods.[2, 3] To make better use of AgNP in wide applications, AgNP are commonly dispersed and immobilized on graphene sheets to avoid their aggregation. Graphene nanomaterials, mainly including graphene oxide (GO) and reduced graphene oxide (rGO), are considered as the ideal 2D support for metal nanoparticles because of their large surface area, extreme mechanical stiffness, abundant surface functional groups, and

superior electronic and thermal conductivity.[2] Nowadays, much concern has been paid on the synthesis and application of AgNP/graphene nanocomposites due to their ease of scale-up production and synergistically enhanced and novel properties in comparison with individual components such as stacking prevention of graphene sheets, enhanced electronic conduction, more controlled Ag^+ release for antimicrobial and highly efficient adsorbent.[4-17]

So far, the general approach for the synthesis of AgNP/graphene nanocomposites is the in-site reduction of Ag^+ ions on graphene sheets[13-17] or loading the premade-in-water AgNP on graphene sheets in the aqueous media.[5-7] However, these water-base methods have experienced difficulty in controlling the particle size and dispersity of AgNP on graphene sheets due to the ionic interactions between the growing nuclei.[18] Besides, the combination between AgNP and graphene is often obtained by intermolecular weak interactions including physical adsorption and electrostatic binding,[19] which may lead to the detachment or reaggregation of AgNP on graphene sheets. Contrarily, AgNP synthesized in organic phase can maintain the predefined size and shape with narrow dispersity.[20] In this regard, recent studies have presented the two-phase interface-assembling method to prepare high-quality AgNP/GO nanocomposite by using GO as a phase transfer agent.[4, 19, 21] But this preparation process was time-consuming and low-efficient probably due to the very limited ability of GO for phase-transferring and anchoring AgNP. Therefore, it is highly desirable to develop a novel preparation method for addressing all these structural factors of AgNP/graphene nanocomposite to further improve its performance.

For the utility in biological systems, AgNP/GO nanocomposite is normally stabilized and modified by amino acid, proteins and other biomolecules.[22, 23] Cysteine, a special biomolecule with multifunctional groups of -SH, -NH_2, and -COOH, may effect as a organic-to-water phase transfer agent because it can replace the hydrophobic groups bound to the AgNP surface via metal-thiolate bond formation, meanwhile render the AgNP water-soluble with its terminally polar functional groups.[24-26] Besides, the -NH_2 group present in cysteine may help for the immobilization of AgNP onto GO sheets through chemisorption interaction such as amido linkage.[27-29] The preparation of cysteine capped-AgNP/graphene nanocomposite has been reported previously,[5-7] where cysteine was used to modify the preformed citrate-stabilized AgNP and then link to graphene sheets and simultaneously reduce GO to rGO. However, these all-water-base preparation methods always yield the undesirable large and dispersive AgNPs (40~70 nm), weak bonding between AgNP and graphene sheet, and low nanoparticle loading efficiency, which would responsible for their moderate performances. In this work, we propose a facile, rapid, phase transfer (PT)-assisted process for preparing AgNP/GO nanocomposite, by tactfully using cysteine as a high-effective phase transfer agent for AgNP movement from toluene to water and subsequently as a covalent linkage for immobilizing AgNP on GO. It is worth highlighting that the as-prepared cysteine stabilized-AgNP/GO (*c*-Ag/GO) nanocomposite concurrently features high nanoparticle loading efficiency, small particle size and monodispersity, strong binding force, and good water dispersibility. These outstanding features confer *c*-Ag/GO an enlarged active surface, ease access of the target substance, good long-term stability, and hence a promising potential for a variety of bio-applications. As the illustrations of application, *c*-Ag/GO and its derivatives *c*-Ag/rGO were used for antibiosis and biosensing, respectively. Compared with the previous reported water-base or two-phase AgNP/graphene nanocomposites, the *c*-Ag/GO exhibits the remarkably improved antibacterial activity and electrochemical biosensing performance.

2. Methods

2.1. Materials

Natural graphite powder (325 meshes) was purchased from Qingdao Huatai Lubricant Sealing S&T Co. Ltd (Qingdao, China). Tetraoctylammonium bromide (TOAB) (98%) and uric acid (UA) (99%) were bought from Alfa Aesar Chemical Co., Ltd (Tianjing, China). $AgNO_3$ were supplied by Sinopharm Chemical Reagent Co., Led (Shanghai, China). Cysteine was obtained from Shanghai Sanpu Chemical Co., Ltd (Shanghai, China). All the chemicals were used as received without further purification.

2.2. PT-assisted synthesis of c-Ag/GO nanocomposite

2.2.1. The synthesis of TOAB-stabilized AgNP in toluene. The synthesis of TOAB-stabilized AgNP in toluene referred to the procedures in the published literature.[30] In brief, 30 mL $AgNO_3$ aqueous solution (30 mM) and 25 mL freshly prepared $NaBH_4$ aqueous solution (0.4 M) were added to 80 mL TOAB toluene solution (25 mM) with continuous stirring at room temperature. The as-prepared TOAB-stabilized AgNP in toluene was subsequently washed with H_2SO_4, NaOH, and deionized water (three times), and then dried over anhydrous Na_2SO_4 and finally re-dispersed in toluene.

2.2.2. The synthesis of cysteine-stabilized AgNP in water. For fabricating cysteine-stabilized AgNP (*c*-Ag), 0.1 M cysteine aqueous solution (80 mL) was added to the as-prepared TOAB-stabilized AgNP toluene solution (1 mg/mL, 40 mL) under vigorous stirring. Phase transfer of AgNP from toluene to water was initiated under vigorous shaking, with complete transfer across the phase boundary in a few minutes.

Almost all AgNP were transferred into water phase through metal-thiolate bond formation between Ag and cysteine. Solid cysteine could also be added directly to the toluene solution to precipitate the AgNP, which could then be resuspended in water.

2.2.3. The immobilization of c-Ag onto GO sheets in water. GO was prepared from natural graphite powder by oxidation with $KMnO_4$ in concentrated H_2SO_4 according to the modified Hummer's method.[31] 20 mL *c*-Ag aqueous solution (1 mg/mL) was mixed with 10 mL GO aqueous solution (0.5 mg/mL) under constant stirring at 60 °C for 1 h. The obtained products were separated by centrifuging, washed with anhydrous alcohol and deionized water for three times successively, and finally re-dispersed in deionized water to obtain *c*-Ag/GO nanocomposite.

2.3. One-pot synthesis of Ag/GO nanocomposite

For the comparison, one-pot AgNP/GO nanocomposite was also prepared. 10 mL homogeneous suspension of GO (0.5 mg/mL) was mixed with 20 mL $AgNO_3$ aqueous solution (31.5 mg $AgNO_3$). Then 0.1 M NaOH was added to the above mixture and vigorously stirred for 1 h at 60 °C. the products were separated by centrifuging, washed with anhydrous alcohol and deionized water successively for three times, and finally re-dispersed in deionized water to obtain one-pot Ag/GO nanocomposite.

To verify the different binding force between AgNP and GO, *c*-Ag/GO and one-pot Ag/GO were sonicated in an ultrasonic generator (KQ2200DB, Kunshan Ultrasonic Instrument Co., Ltd., China, 300 W, 40 kHz) at ambient temperature for 2 h.

2.4. Characterizations

X-ray photoelectron spectra were carried out on a PHI 5300 X-ray Photoelectron Spectrometer (PE, America). Fourier transform infrared spectra (FTIR) were carried out on a Spectrum GX FTIR system (PerkinElmer). UV-vis absorption spectra were recorded on a UV-2401PC UV-vis recording spectrophotometer (Shimadzu, Japan). The morphology of as-prepared products was observed by transmission electron microscopy (TEM, JEM2010) with an acceleration voltage of 200 kV (the EDS as the attached facilities of JEM2010). Raman spectra were recorded on a Renishaw Raman system model 1000 spectrometer equipped with a CCD detector.

2.5. Antibacterial activity test

Gram negative bacterial strain *E. coli* was used as an experimental strain, and the Luria-Bertani (LB) medium (10 g/L tryptone, 5 g/L yeast extract and 5 g/L NaCl) was used for cultivating the bacterial. All plates, flasks and materials were sterilized in an autoclave at 121 °C for 20 min before experiments. For antibacterial activity test, 5 mL of bacteria-LB nutrient mixture (10^7 CFU/mL) were added into the Erlenmeyer flask containing 45 mL saline solution and different concentration of antimicrobials. The mixture with pH value adjusted to 7.0 was incubated for 24 h at 37 °C under 250 rpm shaking speed in the shaking incubator. No antimicrobial was added to another Erlenmeyer flask containing 5 mL of bacteria-LB nutrient and 45 mL saline solution, which was served as a control sample. Subsequently, a certain amount of bacteria suspension was diluted 100 times to make the final bacteria concentration to be 10^4 CFU/mL. LB medium containing agar base (20 g/L) was treated by autoclaving process firstly. After cooling down to about 50 °C, the agar solutions were poured into culture plates (7.5 cm in diameter). After cooled down to room temperature, 100 μL diluted bacteria suspension was spread on a culture plate. All the culture plates were incubated for 24 h at 37 °C in the thermostat to count and record the number of bacterial colonies. The numbers of viable bacterial cells in the above cultures were analyzed using the colony forming units (CFU) counting to determine the E. coli viability in accordance with the Eq. (1)

$$E.coli \text{ viability}(\%) = \mathrm{B}/A \times 100\% \quad (1)$$

where A is the number of bacterial colonies counted from control experiment, and B is the number of bacterial colonies counted from each antibacterial experiment.

2.6. Electrochemical detection of UA

The glassy carbon electrode (GCE, Φ=3 mm) was successively polished by 0.3 μm and 0.05 μm alumina slurry, and rinsed thoroughly with ethanol and water each for 5 min, then dried under a nitrogen stream. 10 μL of the suspension containing *c*-Ag/GO nanocomposite (1 mg/mL) was dropped onto the surface of GCE and dried in air. Electrochemical measurements were carried out on an electrochemical workstation (CHI660A, CH Instructions, Shanghai) at room temperature. The employed three-electrode cell system consisted of modified GCE as working electrode, saturated calomel electrode (SCE) as reference electrode and platinum sheet as counter electrode. All electrochemical experiments were performed using a 10 mL electrolyte solution. The electrochemical reduction of *c*-Ag/GO was performed at a constant potential of -0.9 V *vs.* SCE for 1000 s in a 0.01 M phosphate buffer solution (PBS, pH=4.2).[32] The as-prepared *c*-Ag/rGO-modified GCE was rinsed with water and dried for the following experiment use.

Prior to electrochemical measurements of UA, the electrolyte solution was purged with high purity nitrogen gas for about 10 min to remove dissolved oxygen, and then the working electrode was immersed in the electrolyte solution to preconcentrate UA on the electrode surface for 3 min under magnetic stirring. Cyclic voltammetry (CV) was used to evaluate the electrochemical behavior of c-Ag/rGO

modified GCE in the aqueous solution of 5 mM $K_4Fe(CN)_6$ and 1 M KCl with the potential range of -0.2~0.7 V *vs.* SCE at a potential scan rate of 50 mV/s. Differential pulse voltammetry (DPV) measurements were performed in 0.05 M PBS (pH = 7.0) solution containing 5 mM UA with step height of 4 mV, pulse height of 25 mV and frequency of 10 Hz to determine the electrochemical activity of *c*-Ag/rGO-modified GCE for UA. Linear sweep voltammetry (LSV) was recorded in 0.05 M PBS containing 1 mM UA with the range from 0.1 to 0.7 V *vs.* SCE at scan rate of 10~200 mV/s. The amperometry traces was recorded on *c*-Ag/rGO polarized at 0.38 V vs. SCE upon successively adding UA into 0.05 M PBS solution under constant stirring. To evaluate the stability, reproducibility and selectivity of the sensor, amperometry method was used at 0.38 V *vs.* SCE in 0.05 mM PBS solution (pH 7.0) containing 20 μM UA. For selectivity, 2 mM of each interference compounds was successively added to the UA detecting solution. The real sample analysis was performed using the standard addition method. Before the measurement, all urine samples collected from the colleagues in our lab were diluted to 1000 times with PBS solution (pH 7.0) without other pre-treatment process. The standard addition method was used for testing recovery rates. Each experiment was repeated 3 times.

3. Results and discussion

3.1. The preparation of c-Ag/GO

The preparation process of *c*-Ag/GO nanocomposite is illustrated in Figure 1. Firstly, TOAB-stabilized AgNP was synthesized in toluene. After an aqueous cysteine solution was added to the as-prepared AgNP toluene mixture, phase transfer of AgNP was initiated under vigorous shaking, with complete transfer across the phase boundary in a few minutes (Figure 1a and 1b). The transfer yield is high with very few AgNP remaining in the toluene phase. It is proposed that the ligand exchange happens on phase transfer process through metal-thiolate bond formation due to the high affinity of sulfur for Ag.[26, 33] Comparing the XPS spectra of AgNP before and after phase transfer identified this ligand exchange process, with the upshift of binding energy of Ag 3d and disappearance of the Br 3d peak after phase transfer (see Supporting Information, Figure S1). Afterwards, the cysteine-stabilized AgNP were tightly immobilized onto GO sheets through covalent bond via mixing and stirring in the aqueous solution (Figure 1c), which will be characterized hereinafter. The finally obtained *c*-Ag/GO nanocomposite showed the excellent water dispersion stability, with no signs of coagulation after three-month standing (Figure 1d).

This preparation process of *c*-Ag/GO was also monitored by UV-vis spectra (Figure 2). AgNP has a distinct surface plasmon resonance (SPR) absorption at 388 nm in toluene (Figure 2a). After PT, the SPR wavelength of AgNP in water (389 nm) slightly red-shifted, which could arise from the combined effect of the change in refractive index of the solvent (from toluene to water) and adsorbed ligand molecules (from TOAB to cysteine).[33]

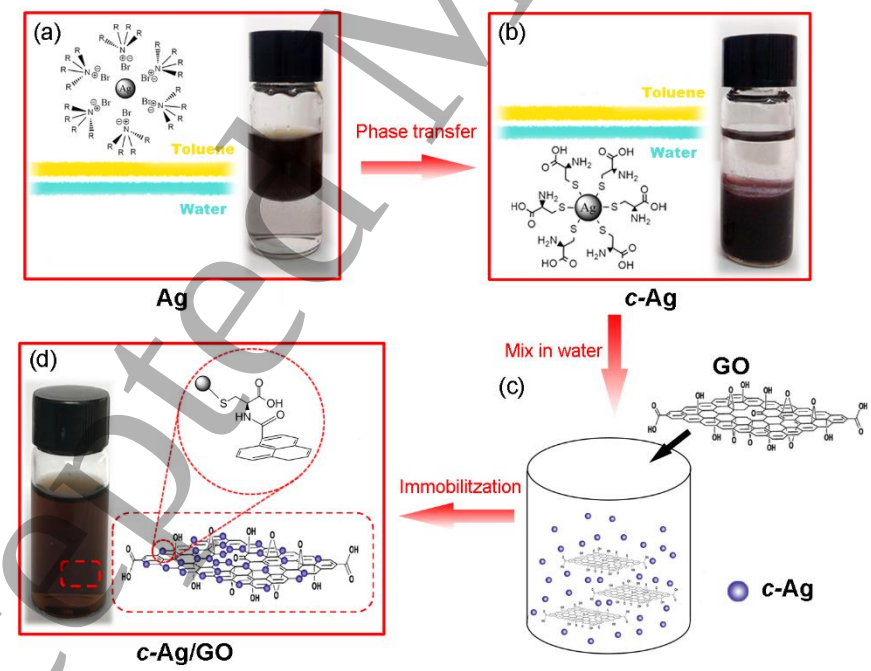

Figure 1. Schematic illustration for the preparation of *c*-Ag/GO nanocomposite: (a) TOAB-stabilized AgNP in toluene before phase transfer, (b) cysteine stabilized-AgNP in water after phase transfer, (c) the immobilization of *c*-Ag onto GO in water, (d) graphic presentation of covalent linkage between *c*-Ag and GO, and photo of stable and well-dispersed *c*-Ag/GO nanocomposite after stored in water for 3 months.

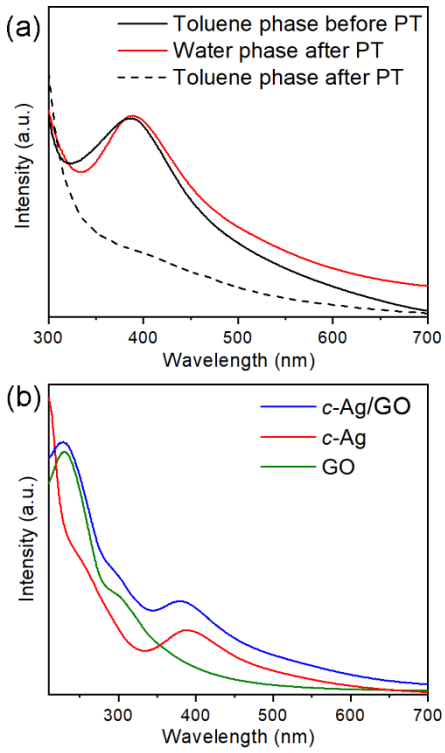

Figure 2. (a) UV-vis absorption spectra of water and toluene phases before and after PT, (b) UV-vis absorption spectra of GO, *c*-Ag and *c*-Ag/GO in water.

Meanwhile, the almost disappeared SPR peak for toluene solution indicated complete transfer of AgNP into water. From Figure 2b, the formed *c*- Ag/GO nanocomposite exhibits the two peaks at 230 and 300 nm corresponding to the characteristic absorptions of GO,[9] and one peak at 382 nm belonging to the SPR of AgNP. This SPR peak shows 7 nm blue-shift relative to that for *c*-Ag, possibly due to the presence of GO with large refractive index.[33] Additionally, no broadening of SPR peaks was observed for all tested Ag nanoparticles, reflecting that AgNP can retain their original size and dispersity through the whole transfer and immobilization process.

3.2. The morphologic and structural analysis of c-Ag/GO

The morphology and particle size of *c*-Ag/GO were analyzed by TEM. Figure 3a shows the smooth and wrinkled structure of uncovered GO sheets. After combined with *c*-Ag, the GO sheets are uniformly decorated by AgNP (Figure 3b) with high loading density (the number of AgNP on the unit area of GO sheet ~ 3.59×10^4 per μm^2). From the magnified image of Figure 3c, these immobilized AgNP are well dispersed on GO sheet without any aggregation. By means of statistical counting from TEM image, the average size of AgNP on GO is determined to be 5 ± 0.9 nm, assuming a narrow size dispersity (Figure 3d). The HRTEM image of *c*-Ag/GO shows the clear lattice fringes of nanoparticles as marked in Figure 3e with a *d*-spacing of 0.236 nm, corresponding well to the (111) lattice plane of Ag. The SAED pattern (the inset of Figure 3e) also presents two sets of diffraction spots corresponding to the Ag (111) and (311) lattice planes, demonstrating the crystalline nature of the AgNP on GO. Additionally, the EDS result shows the element composition of *c*-Ag/GO containing C, O, Ag and S elements, and Cu element here comes from the copper mesh for TEM characterization, verifying that *c*-Ag are successfully deposited on GO sheets (Figure 3f).

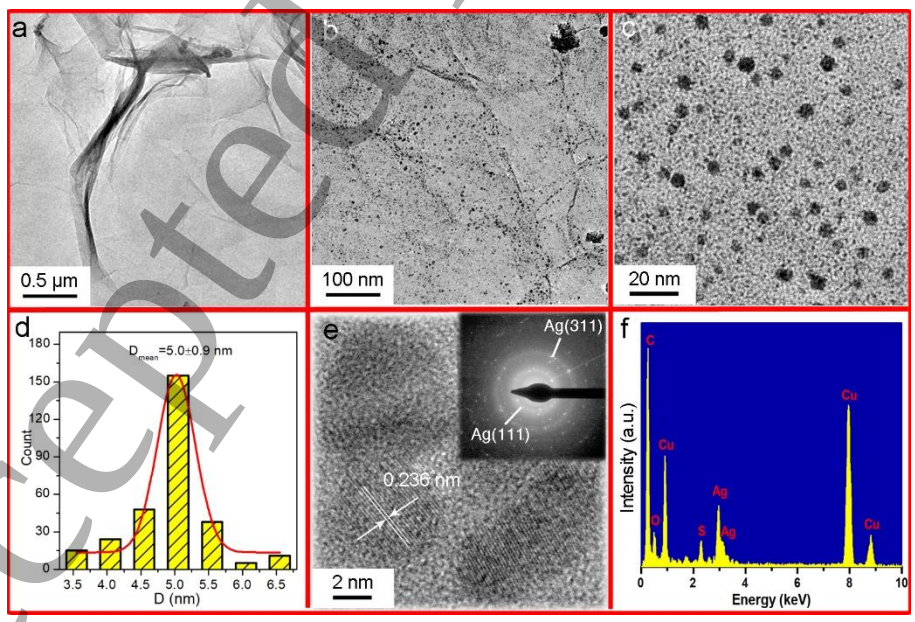

Figure 3. TEM images of (a) GO and (b), (c) *c*-Ag/GO, (d) the particle size distribution of AgNP on *c*-Ag/GO (N: the total amount of nanoparticles for statistical counting), (e) HRTEM image and SAED pattern (inset) of *c*-Ag/GO, (f) EDS of *c*-Ag/GO.

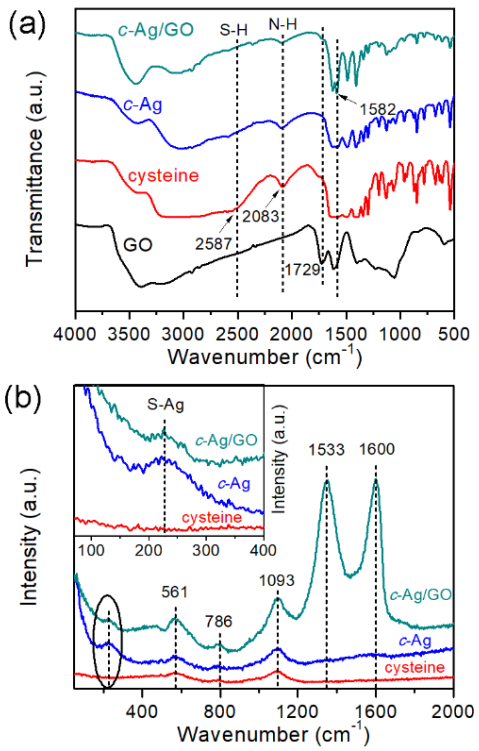

Figure 4. (a) FTIR spectra of GO, cysteine, *c*-Ag and *c*-Ag/GO. (b) Raman spectra of cysteine, *c*-Ag and *c*-Ag/GO. Inset: the amplifying Raman spectra in the wavenumber range from 60 to 400 cm^{-1} of Figure 4b.

The chemical structure of *c*-Ag/GO was probed by FTIR and Raman spectra in Figure 4. From Figure 4a, *c*-Ag and *c*-Ag/GO almost inherit the FTIR spectrum profile of cysteine, proving the presence of cysteine in *c*-Ag and *c*-Ag/GO as a capping and bridging agent. Specifically, the S-H vibration band at 2587 cm^{-1} and N-H stretching band at 2083 cm^{-1} are clearly seen in the FTIR spectrum of free cysteine molecule.[34] The vanishment of the S-H vibration band in the spectra of *c*-Ag and *c*-Ag/GO can be attributed to formation of metal-thiolate linkage between AgNP and capping cysteine molecule.[34, 35] Also, the obvious decrease in intensity of N-H stretching band in the spectrum of *c*-Ag/GO presumably suggests that there exists a certain bonding interaction between *c*-Ag and GO. Further comparing with GO, the disappearance of band at 1729 cm^{-1} (carboxyl group in GO) and appearance of new band at 1582 cm^{-1} (secondary amide group) in the spectrum of *c*-Ag/GO demonstrate the formation of amide bond between cysteine and GO,[27, 36] reflecting that the cysteine-stabilized AgNP were immobilized on GO sheets by amide bond. The Raman spectrum of *c*-Ag/GO in Figure 4b shows three characteristic peaks at 561, 786 and 1093 cm^{-1}, resulting from the C-C stretching, O=C-O bending and C-H bending in cysteine component respectively,[37] and two strong peaks assigned to D (1355 cm^{-1}) and G band (1600 cm^{-1}) of GO,[38] indicating cysteine and GO have been included in the *c*-Ag/GO nanocomposite. Furthermore, a weak peak at 225 cm^{-1} can be detected for *c*-Ag and *c*-Ag/GO (inset), revealing the formation of S-Ag bond between cysteine and AgNP,[25, 39] which is consistent with the result of FTIR.

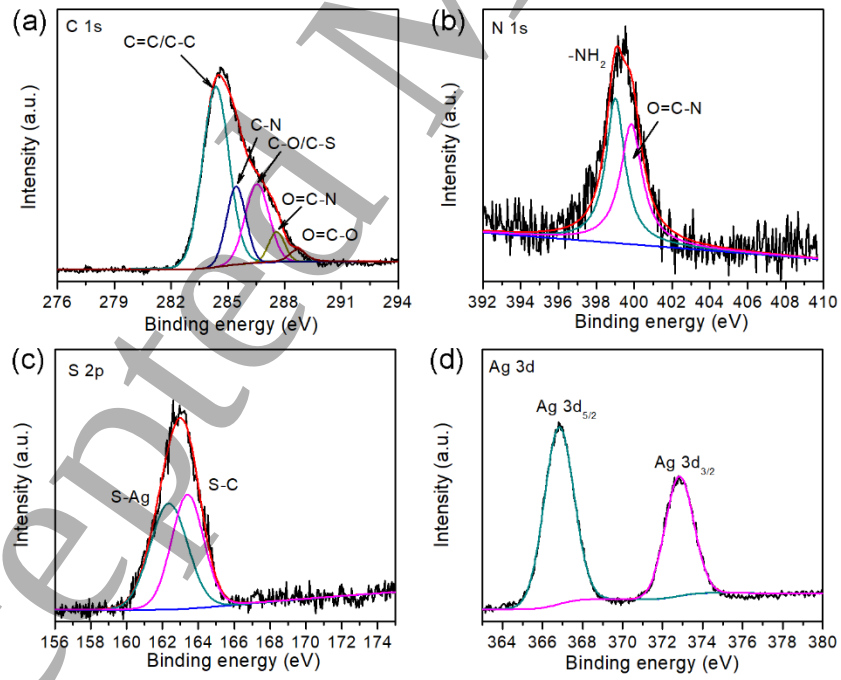

Figure 5. High resolution XPS of C 1s, N 1s, S 2p and Ag 3d over *c*-Ag/GO nanocomposite.

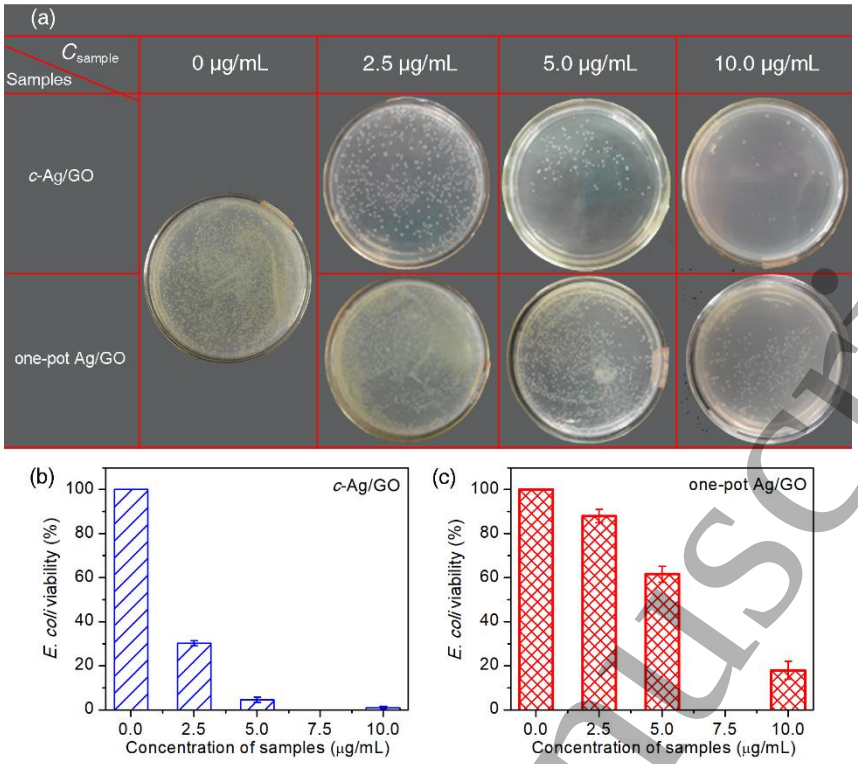

Figure 6. (a) Photos of *E. coli* bacteria colonies cultivated on agar plates after contact with the antimicrobials of different concentrations. *E. coli* viability after treated by (b) *c*-Ag/GO and (c) one-pot Ag/GO of different concentrations.

The elemental composition and valence state of *c*-Ag/GO were further investigated by XPS measurement. C 1s core-level spectrum of *c*-Ag/GO in Figure 5a consists of five component peaks, which are related to the different carbon bond structures in GO and cysteine, including C-C/C=C (284.4 eV), C-N (285.5 eV,), C-O/C-S (286.6 eV), O=C-N (287.6 eV, assigned to amide linkage) and O=C-O (288.7 eV).[27] N 1s spectrum in Figure 5b can be decomposed into two components, and the binding energy at 399.0 eV is assigned to -NH_2 group in cysteine and that at 400.1 eV to O=C-N group in the amide linkage between cysteine and GO.[40] Moreover, the deconvolution of S 2p spectrum (Figure 5c) results in two subpeaks at 162.4 and 163.4 eV, which are ascribed to S-Ag and S-C bonds respectively,[41, 42] indicating of the formation of metal-thiolate linkage between AgNP and capping cysteine molecule. Ag 3d spectrum in Figure 5d shows two feature peaks at 368.1 eV (Ag $3d_{5/2}$) and 374.1 eV (Ag $3d_{3/2}$) with the binding energy separation of 6.0 eV, which is characteristic of metallic Ag,[43, 44] indicating the successful anchoring of AgNP on GO.

The above results unveil that the cysteine biomolecule plays a critical role both in rapid phase transfer of AgNP from toluene to water and subsequently fixing AgNP on GO, which is totally different from the functions of cysteine in the previous reported cysteine capped-AgNP/graphene nanocomposite [5-7] due to the distinct preparation process. Here, the resultant *c*-Ag/GO nanocomposite enjoys high nanoparticle loading density, improved particle size and monodispersity, as well as the excellent water dispersibility, which would render it a promising potential in a variety of biological applications. To further highlight the advantages of the preparation method for *c*-Ag/GO, the control sample Ag/GO was also prepared by conventional one-pot method. As seen in Figure S2a and S2b, the average size of AgNP in one-pot Ag/GO is 14±6 nm, showing the relatively larger particle size and wider size dispersity than *c*-Ag/GO. This structural difference between two samples was also reflected from UV-vis spectra in Figure S2d, with one-pot Ag/GO producing a red-shifted and broadened SPR absorption relative to *c*-Ag/GO. Furthermore, to verify the different binding force between AgNP and GO, these two samples were executed with ultrasonic treatment (US) under the same conditions and their TEM images and UV-vis spectra after US are displayed in Figure S2c, S2d and Figure S3 respectively. There is no obvious change for *c*-Ag/GO in nanoparticle morphology, loading density, and SPR absorption after US, demonstrating the robust linkage between AgNP and GO originated from covalent bridging effect of cysteine. Contrarily, for one-pot Ag/GO, only limited number of AgNP remain on GO sheet after US, along with the great decrease in SPR intensity, indicating that a large amount of AgNP have been detached from GO during vigorous US treatment due to the weak interaction between AgNP and GO.

3.3. Antibacterial property of c-Ag/GO

Table 1. The comparison of MBC (MIC) against *E. coli* between this work and the literatures.

Materials	Preparation method	Size of AgNPs (nm)	MBC (μg/mL)	Ref.
Ag/rGO	Water-base	1~5	30	[13]
Ag/rGO	Water-base	5	12.5 (MIC)[a]	[14]
Ag/GO	Water-base	9.4±2.8	30	[8]
Ag/GO	Water-base	10~100	47 (MIC)	[16]
Ag/GO	Water-base	5~15	200	[17]
Ag/GO	Water-base	10~70	10 (MIC)	[15]
Ag/GO	Two-phase	7.2	100	[19]
Ag@Fe_2O_3/GO	Two-phase	2~7	43	[21]
Cysteine-Ag/rGO	Water-base	~35	100 (μL)[b]	[6]
Cysteine-Ag/rGO	Water-base	<50	600	[5]
Ag/GO	Water-base	14±6	30	This work
c-Ag/GO	PT-assisted	5±0.9	10	This work

[a] Minimal inhibitory concentration (MIC): the lowest nanomaterial concentration where no bacterial growth was visualized. Generally, MBC is greater than or close to MIC.[8] [b] The concentration of antibacterial agent used was not mentioned.

The most important application of AgNP/graphene nanocomposite is as a broad-spectrum antimicrobial. The antibacterial activities of *c*-Ag/GO and one-pot Ag/GO were evaluated via a colony-forming count method by choosing *E. coli* as the model waterborne pathogen. Figure 6 shows the antibacterial activities against *E. coli* over the different concentration of antimicrobials. It can be seen that the number of bacterial colonies decreased with the increase of the concentration of antimicrobials. The antibacterial activity is signified by the minimal bactericidal concentration (MBC) that is defined as the lowest concentration of antimicrobial for killing 99% of bacteria in the culture medium. *c*-Ag/GO exhibits the MBC of 10 μg/mL, which is lower than that of one-pot Ag/GO (30 μg/mL, shown in Figure S4) and even below the MBCs of previously reported AgNP/graphene nanocomposite as listed in Table 1, indicating the remarkably improved antibacterial capability of *c*-Ag/GO. Several possible mechanisms have been proposed for the antibacterial behavior of AgNP-GO nanocomposite, including specific-interaction of AgNP with bacteria, releasing Ag^+ ions to interfere with bacterial DNA, oxidative stress generated by reactive oxygen species (ROS), and a synergetic antibacterial effect of AgNP and GO.[6, 17] Here, the enhanced antibacterial performance of *c*-Ag/GO can be attributed to the following aspects: (1) small and monodispersed AgNP lead to a high antibacterial activity due to the large specific surface area, ease cell penetration, and more ROS generation; (2) the covalent bridging by cysteine between AgNP and GO can provide a good binding stability to avoid the detachment of AgNP during the antibacterial process;[6] (3) the introduction of biomolecule cysteine promotes the compatibility and contact of nanocomposite with bacteria,[5] further improving the antibacterial activity of *c*-Ag/GO.

3.4. UA detection performance of c-Ag/GO

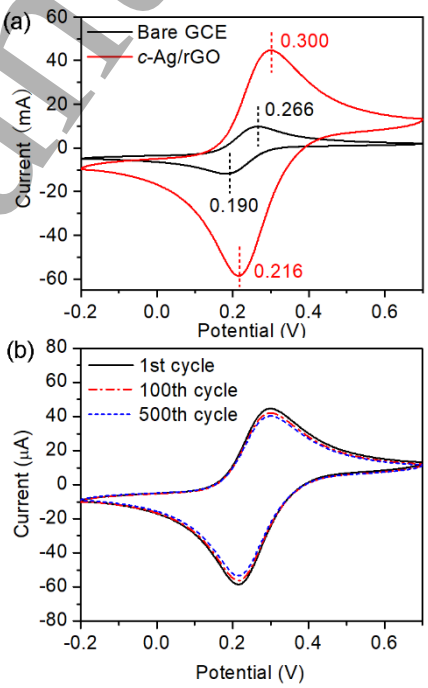

Figure 7. (a) CV curves of bare GCE and *c*-Ag/rGO in the aqueous solution of 5 mM $K_4Fe(CN)_6$ and 1 M KCl at a potential scan rate of 50 mV/s. (b) Stability of CV curves of *c*-Ag/rGO in the same solution.

As an example of another potential application for AgNP/graphene nanocomposite, the biosensor based on *c*-Ag/rGO modified glassy carbon electrode (GCE) for detecting uric acid was investigated. The *c*-Ag/rGO modified electrode was obtained by *in-site* electrochemical reduction of *c*-Ag/GO modified electrode, and its electrochemical behavior was firstly evaluated in the aqueous solution of

$K_4Fe(CN)_6$ and KCl. From Figure 7a, both CV cycles of *c*-Ag/rGO and bare GCE show a pair of oxidation and reduction peaks owing to Fe^{3+}/Fe^{2+}. It is clear that the CV peak current of *c*-Ag/rGO are much higher than that of bare GCE, revealing the improved electrochemical activity of modified electrode. Moreover, the redox peak separation of *c*-Ag/rGO (84 mV) is just slightly bigger than that of bare GCE (76 mV), implying the small charge transport resistance of modified layer attributed to the interconnected conductive rGO sheets and tightly binded individual AgNP. Additionally, Figure 7b shows that *c*-Ag/rGO almost retains the original shape of CV curve after multi-cycle CV measurements, demonstrating its good electrochemical stability, which is probably related to strong binding force between AgNP and rGO via cysteine bridging effect.

As a primary product for purine metabolism, the abnormal concentration levels of UA in urine and serum will lead to the symptoms of gout and hyperuricemia.[45-47] Thus, the detection of UA from the simulated humoral environment is of great significance. Figure 8a shows the DPV curves of *c*-Ag/rGO and bare GCE in 0.05 M PBS (pH = 7.0) solution containing 5 mM UA. An oxidation peak due to UA was detected at 0.38 V *vs.* SCE for two electrodes, while the peak current on *c*-Ag/rGO at this potential is greatly higher than that on bare GCE, indicating that *c*-Ag/rGO nanocomposite exhibit a significantly enhanced electrocatalytic activity for UA oxidation, which may results from the enlarged, activated surface of *c*-Ag/rGO for fully contacting with UA molecules and its good conductivity for electron transfer. The electrocatalytic oxidation of UA on *c*-Ag/rGO was also tested at different scan rates as depicted in Figure 8b. The oxidation peak current increases linearly with the square root of the scan rate in the range of 10 to 200 mV/s, suggesting that electrochemical reaction process is controlled by the diffusion of UA, and further proving the fast charge transfer characteristic of the modified layer. The amperometry traces in Figure 8c was recorded on *c*-Ag/rGO polarized at 0.38 V *vs.* SCE upon successive adding UA into PBS solution under constant stirring. The anodic current increases abruptly after each addition of UA, and reaches a plateau in a very short time (< 0.5 s), indicating a quick and stable response to UA amount change. The limitation of detection (LOD) for *c*-Ag/rGO measured at a signal-to-noise ratio (S/N) of 3 is 0.025 μM (inset of Figure 8c). In addition, the current response of this sensor shows a well-defined linear relationship to the concentration of UA in the range of 0.025~50 μM (R=0.998) and 200~2250 μM (R=0.999) with sensitivity of 5.76 and 0.98 (μA/mM) respectively (Figure 8d). All the above values obtained from *c*-Ag/rGO are found to greatly surpass those of previously reported noble-metal-loaded-graphene modified electrodes for detecting UA as listed in Table 2, evidencing the advantages such as high sensitivity, low LOD and wide linear range of *c*-Ag/rGO for UA detection.

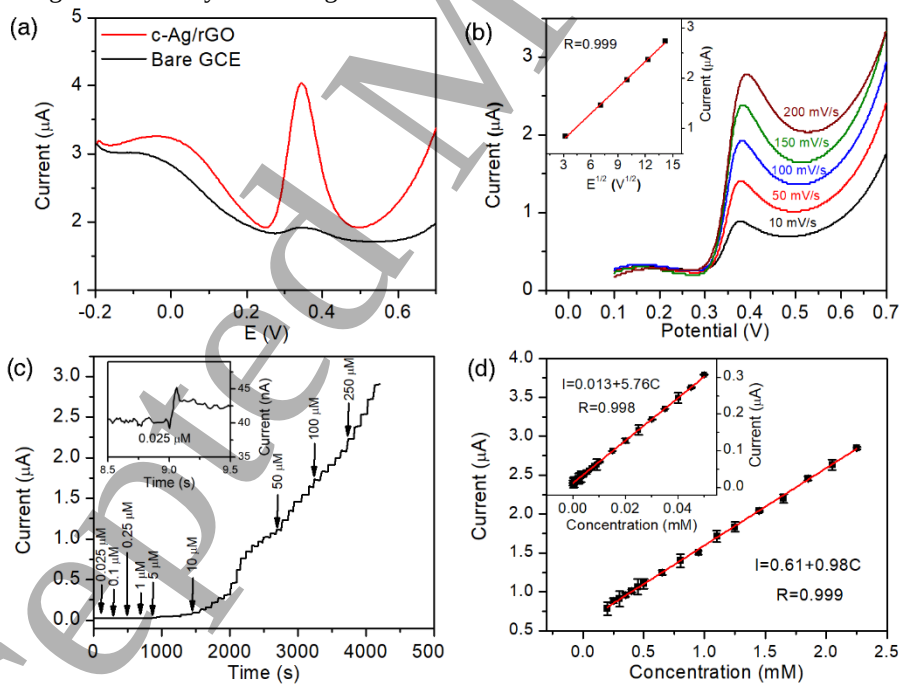

Figure 8. (a) DPV curves of bare GCE and *c*-Ag/rGO modified GCE in 0.05 M PBS (pH=7.0) solution containing 5 mM UA. (b) LSV curves of *c*-Ag/rGO at scan rate of 10~200 mV/s in PBS containing 1 mM UA, Inset: plots of peak current *vs.* the square root of the scan rate. (c) The amperometry traces recorded on *c*-Ag/rGO polarized at 0.38 V upon successive adding UA into PBS solution under constant stirring. Inset: the current response at the LOD concentration of UA. (d) The calibration curves at a concentration range of 0.025~50 (the inset) and 200~2250 μM.

The *c*-Ag/rGO sensor was further investigated by amperometry method at 0.38 V *vs.* SCE. Five parallel *c*-Ag/rGO electrodes were made to evaluate the reproducibility, and their current responses to UA (20 μM) were almost the identical with the relative standard deviation (RSD) of 2.07% (Figure S5a), confirming that the preparation method for *c*-Ag/rGO was highly reproducible. One *c*-Ag/rGO electrode stability was estimated by measuring its current responses to UA (20 μM) repeatedly for 10 days. There is no obvious current change for these repeated measurements and the RSD was found to be 3.94% (Figure S5b), indicative of the excellent stability of *c*-Ag/rGO electrode, which may results from the combined factors including the strong binding between AgNP and rGO, the anti-fouling behavior of cysteine on the electrode surface,[48] and the electrochemical stability of cysteine protective AgNP during detection process.[49] To investigate the selectivity of the sensor for detecting UA, several possible interference molecules involving ascorbic acid (AA), dopamine (DA), glycine, glucose, lysine, $NaNO_3$, KCl, Na_2SO_4 and acetaminophen were added successively into the UA detecting solution, and no significant current interference was observed (Figure S6), demonstrating that *c*-Ag/rGO is highly selective to sensing UA. Finally, the *c*-Ag/rGO electrode was used in real urine sample analysis by standard addition method, and the results were listed in Table S1. The recovery rates of the spiked samples are checked in a range from 97.67% to 104.00%, confirming the reliability of *c*-Ag/rGO modified electrode for UA determination in real urine samples.

4. Conclusion

c-Ag/GO nanocomposite was prepared by using cysteine as a high-effective phase transfer agent for moving AgNP synthesized in toluene to water and subsequently as a covalent linkage for fixing AgNP on GO. FTIR and XPS results demonstrate that the bridging effect of cysteine biomolecule between AgNP and GO was achieved via the formation of S-Ag and amide bonds. As the illustrations of application, *c*-Ag/GO and its derivatives *c*-Ag/rGO were used for antibiosis and biosensing respectively. The antimicrobial *c*-Ag/GO shows the high antibacterial activity against *E. coli* with the minimal bactericidal concentration of 10 μg/mL. And the biosensor based on *c*-Ag/rGO exhibits the rapid and sensitive response for uric acid detection with the detecting limit of 0.025 μM, sensitivity of 5.76 μA/mM, and wide linear range of 0.025~2250 μM. The comparative analysis with relevant nanocomposites also demonstrates the advantages of *c*-Ag/GO in these applications. These outstanding performances of *c*-Ag/GO can be attributed to its superior features including high nanoparticle loading efficiency, small particle size and monodispersity, strong binding force, and good water dispersibility. Besides, the developed phase-transfer-assisted method provides a new avenue for preparing water-soluble and size-controlled metal nanoparticle immobilized graphene nanocomposites for broad applications.

Table 2 The comparison of linear range, LOD and sensitivity for UA detection from literatures and this work.

Electrode material	Linear range (μM)	LOD (μM)	Sensitivity (μA/μM)	Ref.
Ag/rGO	10~800	8.2	0.39	[50]
Ag/rGO	35~300	0.30	0.26	[47]
Au/rGO	2~62	0.2	(~0.066)	[51]
Au/GO	8.8~53	1.8	0.5	[32]
Pt/rGO	0.05~11.85	0.05	0.4119	[52]
Pt/rGO	10~130	0.45	0.042	[53]
Pd-Ag/rGO	1.0~150	0.081	(~0.05)	[54]
Au-Pt/rGO	0.125~82800	0.0407	-0.6913	[55]
Ag/Zeolite	0.05~0.7	0.0251	19.2975	[56]
c-Ag/rGO	0.025~50 200~2250	0.025	5.76, 0.98 (μA/mM)	This work

Acknowledgements

This work was financially supported by Foundation of Jiangxi Provincial Department of Education (GJJ190988), Natural Science Project of Jiangxi University of Technology (ZR1811).

References

[1] Liu H, Zhong L, Yun K and Samal M 2016 Synthesis, characterization, and antibacterial properties of silver nanoparticles-graphene and graphene oxide composites *Biotechnology and Bioprocess Engineering* **21** 1-18

[2] He K, Zeng Z, Chen A, Zeng G, Xiao R, Xu P, Huang Z, Shi J, Hu L and Chen G 2018 Advancement of Ag-Graphene Based Nanocomposites: An Overview of Synthesis and Its Applications *Small* **14** e1800871

[3] Li J, Liu C-y and Liu Y 2012 Au/graphene hydrogel: synthesis, characterization and its use for catalytic reduction of 4-nitrophenol *Journal of Materials Chemistry* **22**

[4] Xiao Y, Liu J, Lin Y, Lin W and Fang Y 2017 Novel graphene oxide-silver nanorod composites with enhanced photocatalytic performance under visible light irradiation *Journal of Alloys and Compounds* **698** 170-7

[5] Fathalipour S, Pourbeyram S, Sharafian A, Tanomand A and Azam P 2017 Biomolecule-assisted synthesis of Ag/reduced graphene oxide nanocomposite with excellent electrocatalytic and antibacterial performance *Materials Science and Engineering C* **75** 742-51

[6] Chandraker K, Nagwanshi R, Jadhav S K, Ghosh K K and Satnami M L 2017 Antibacterial properties of amino acid functionalized silver nanoparticles decorated on graphene oxide sheets *Spectrochimica Acta Part A: Molecular and Biomolecular Spectroscopy* **181** 47-54

[7] Sahu D, Sarkar N, Sahoo G, Mohapatra P and Swain S K 2019 Nano silver imprinted graphene oxide as catalyst in reduction of 4 - nitrophenol *Journal of Physical Organic Chemistry* **32**

[8] de Moraes A C, Lima B A, de Faria A F, Brocchi M and Alves O L 2015 Graphene oxide-silver nanocomposite as a promising biocidal agent against methicillin-resistant Staphylococcus aureus *International Journal of Nanomedicine* **10** 6847-61

[9] Li F and Dong B 2019 Facile two-step synthesis of Ag nanoparticles dispersed on N, S co-doped RGO for highly efficient plasmonic photocatalytic water purification *Catalysis Communications* **119** 42-5

[10] Tan S, Wu X, Xing Y, Lilak S, Wu M and Zhao J X 2020 Enhanced synergetic antibacterial activity by a reduce graphene oxide/Ag nanocomposite through the photothermal effect *Colloids Surf B Biointerfaces* **185** 110616

[11] Li Y, Chen C, Cao R, Pan Z, He H and Zhou K 2020 Dual-atom Ag2/graphene catalyst for efficient electroreduction of CO2 to CO *Applied Catalysis B: Environmental* **268**

[12] Li Z, Wang X, Yin Z, Zhao J, Song M, Wu Z, Li H and Wang X 2020 Ag nanoparticles decorated N/S dual-doped graphene nanohybrids for high-performance asymmetric supercapacitors *Carbon* **161** 726-35

[13] He G-Y, Dai W, Zhao Y-T, Chen Q, Sun X-Q, Chen H-Q and Wang X 2013 A facile synthesis of Ag@graphene-nanosheet composite with enhanced antibacterial activity and acceptable environmental safety *Monatshefte für Chemie - Chemical Monthly* **145** 3-10

[14] Xu W-P, Zhang L-C, Li J-P, Lu Y, Li H-H, Ma Y-N, Wang W-D and Yu S-H 2011 Facile synthesis of silver@graphene oxide nanocomposites and their enhanced antibacterial properties *Journal of Materials Chemistry* **21** 4593–7

[15] Zhang D, Liu X and Wang X 2011 Green synthesis of graphene oxide sheets decorated by silver nanoprisms and their anti-bacterial properties *Journal of Inorganic Biochemistry* **105** 1181-6

[16] Kulshrestha S, Qayyum S and Khan A U 2017 Antibiofilm efficacy of green synthesized graphene oxide-silver nanocomposite using Lagerstroemia speciosa floral extract: A comparative study on inhibition of gram-positive and gram-negative biofilms *Microbial Pathogenesis* **103** 167-77

[17] Song B, Zhang C, Zeng G, Gong J, Chang Y and Jiang Y 2016 Antibacterial properties and mechanism of graphene oxide-silver nanocomposites as bactericidal agents for water disinfection *Archives of Biochemistry and Biophysics* **604** 167-76

[18] Sastry M 2003 Phase transfer protocols in nanoparticle synthesis *Current Science* **85** 1735-45

[19] Liu L, Liu J, Wang Y, Yan X and Sun D D 2011 Facile synthesis of monodispersed silver nanoparticles on graphene oxide sheets with enhanced antibacterial activity *New Journal of Chemistry* **35** 1418–23

[20] Yang J, Lee J Y and Ying J Y 2011 Phase transfer and its applications in nanotechnology *Chem Soc Rev* **40** 1672-96

[21] Gao N, Chen Y and Jiang J 2013 Ag@Fe2O3-GO nanocomposites prepared by a phase transfer method with long-term antibacterial property *ACS Applied Materials & Interfaces* **5** 11307-14

[22] Fathalipour S and Abdi E 2016 Glycine-assisted aqueous suspension of reduced graphene oxide/Ag nanocomposite via in situ reduction at room temperature: synthesis and electroactivity behavior *Synthetic Metals* **221** 159-68

[23] Yang B, Liu Z, Guo Z, Zhang W, Wan M, Qin X and Zhong H 2014 In situ green synthesis of silver–graphene oxide nanocomposites by using tryptophan as a reducing and stabilizing agent and their application in SERS *Applied Surface Science* **316** 22-7

[24] Qingquan G, Xinfu M, Yu X, Wei T and Hui Z 2017 Green synthesis and formation mechanism of Ag nanoflowers using l-cysteine and the assessment of Ag nanoflowers as SERS substrates *Colloids and Surfaces A: Physicochemical and Engineering Aspects* **530** 33-7

[25] Nidya M, Umadevi M and Rajkumar B J 2014 Structural, morphological and optical studies of l-cysteine modified silver nanoparticles and its application as a probe for the selective colorimetric detection of Hg(2+) *Spectrochimica Acta Part A: Molecular and Biomolecular Spectroscopy* **133** 265-71

[26] Caruso D I G a F 2001 Biological and Physical Applications of Water-Based Metal Nanoparticles

Synthesised in Organic Solution *Chemphyschem* 110-3

[27] Seenivasan R, Chang W J and Gunasekaran S 2015 Highly Sensitive Detection and Removal of Lead Ions in Water Using Cysteine-Functionalized Graphene Oxide/Polypyrrole Nanocomposite Film Electrode *ACS Applied Materials & Interfaces* **7** 15935-43

[28] Muralikrishna S, Sureshkumar K, Varley T S, Nagaraju D H and Ramakrishnappa T 2014 In situ reduction and functionalization of graphene oxide withl-cysteine for simultaneous electrochemical determination of cadmium(ii), lead(ii), copper(ii), and mercury(ii) ions *Anal. Methods* **6** 8698-705

[29] Adegoke O a F, P. B. 2016 L-cysteine-capped core/shell/shell quantum dot-graphene oxide nanocomposite fluorescence probe for polycyclic aromatic hydrocarbon detection *Talanta* **146** 780-8

[30] Caruso D I G a F 2001 Spontaneous Phase Transfer of Nanoparticulate Metals from Organic to Aqueous Media *Angewandte Chemie International Edition* **40** 3001-4

[31] Zhang L and Shi G 2011 Preparation of Highly Conductive Graphene Hydrogels for Fabricating Supercapacitors with High Rate Capability *The Journal of Physical Chemistry C* **115** 17206-12

[32] Wang C, Du J, Wang H, Zou C e, Jiang F, Yang P and Du Y 2014 A facile electrochemical sensor based on reduced graphene oxide and Au nanoplates modified glassy carbon electrode for simultaneous detection of ascorbic acid, dopamine and uric acid *Sensors and Actuators B: Chemical* **204** 302-9

[33] Lista M, Liu D Z and Mulvaney P 2014 Phase transfer of noble metal nanoparticles to organic solvents *Langmuir* **30** 1932-8

[34] Roy M, Mukherjee P, Mandal B P, Sharma R K, Tyagi A K and Kale S P 2012 Biomimetic synthesis of nanocrystalline silver sol using cysteine: stability aspects and antibacterial activities *RSC Advances* **2** 6496–503

[35] Saikat Mandal A G, Neeta Lala, Rajesh Gonnade, Vivek Ganvir, and Murali Sastry 2001 Studies on the Reversible Aggregation of Cysteine-Capped Colloidal Silver Particles Interconnected via Hydrogen Bonds *Langmuir* **17** 6262-8

[36] Pandey C M, Tiwari I, Singh V N, Sood K N, Sumana G and Malhotra B D 2017 Highly sensitive electrochemical immunosensor based on graphene-wrapped copper oxide-cysteine hierarchical structure for detection of pathogenic bacteria *Sensors and Actuators B: Chemical* **238** 1060-9

[37] Pawlukojc A, Leciejewicz J, Ramirez-Cuesta A J and Nowicka-Scheibe J 2005 l-Cysteine: Neutron spectroscopy, Raman, IR and ab initio study *Spectrochimica Acta Part A: Molecular and Biomolecular Spectroscopy* **61** 2474-81

[38] Li F, Zhang L, Chen X, Liu Y L, Xu S G and Cao S K 2017 Synergistically enhanced photocatalytic reduction of CO2 on N-Fe codoped BiVO4 under visible light irradiation *Physical Chemstry Chemical Physics* **19** 21862-8

[39] Lim J K and Joo S-W 2007 Adsorption of seleno-l-cystine on silver electrode surfaces investigated by surface-enhanced Raman scattering *Journal of Electroanalytical Chemistry* **605** 68-72

[40] Gong X, Bi Y, Zhao Y, Liu G and Teoh W Y 2014 Graphene oxide-based electrochemical sensor: a platform for ultrasensitive detection of heavy metal ions *RSC Advances* **4** 24653-7

[41] Battocchio C, Meneghini C, Fratoddi I, Venditti I, Russo M V, Aquilanti G, Maurizio C, Bondino F, Matassa R, Rossi M, Mobilio S and Polzonetti G 2012 Silver Nanoparticles Stabilized with Thiols: A Close Look at the Local Chemistry and Chemical Structure *The Journal of Physical Chemistry C* **116** 19571-8

[42] Zhang H, Niu Y and Hu W 2017 Nitrogen/sulfur-doping of graphene with cysteine as a heteroatom source for oxygen reduction electrocatalysis *Journal of Colloid and Interface Science* **505** 32-7

[43] Han X-W, Meng X-Z, Zhang J, Wang J-X, Huang H-F, Zeng X-F and Chen J-F 2016 Ultrafast Synthesis of Silver Nanoparticle Decorated Graphene Oxide by a Rotating Packed Bed Reactor *Industrial & Engineering Chemistry Research* **55** 11622-30

[44] Bhunia S K and Jana N R 2014 Reduced graphene oxide-silver nanoparticle composite as visible light photocatalyst for degradation of colorless endocrine disruptors *ACS Applied Materials & Interfaces* **6** 20085-92

[45] Ping J, Wu J, Wang Y and Ying Y 2012 Simultaneous determination of ascorbic acid, dopamine and uric acid using high-performance screen-printed graphene electrode *Biosensors and Bioelectronics* **34** 70-6

[46] Yang L, Liu D, Huang J and You T 2014 Simultaneous determination of dopamine, ascorbic acid and uric acid at electrochemically reduced graphene oxide modified electrode *Sensors and Actuators B: Chemical* **193** 166-72

[47] Li S-M, Wang Y-S, Hsiao S-T, Liao W-H, Lin C-W, Yang S-Y, Tien H-W, Ma C-C M and Hu C-C 2015 Fabrication of a silver nanowire-reduced graphene oxide-based electrochemical biosensor and its enhanced sensitivity in the simultaneous determination of ascorbic acid, dopamine, and uric acid *Journal of Materials Chemistry C* **3** 9444-53

[48] Yuqing Zhao J B, Liang Wang, XuHong E, Pengfei Huang, Hongjing Wang, Liying Zhang 2006 Simultaneous Electrochemical Determination of Uric Acid and Ascorbic Acid Using L-Cysteine Self-Assembled Gold Electrode *International Journal of Electrochemstry Science* **1** 363-71

[49] J. Christopher Love L A E, Jennah K. Kriebel, Ralph G. Nuzzo, and George M. Whitesides 2005

Self-Assembled Monolayers of Thiolates on Metals as a Form of Nanotechnology *Chemical Reviews* **105** 1103−69

[50] Kaur B, Pandiyan T, Satpati B and Srivastava R 2013 Simultaneous and sensitive determination of ascorbic acid, dopamine, uric acid, and tryptophan with silver nanoparticles-decorated reduced graphene oxide modified electrode *Colloids Surf B Biointerfaces* **111** 97-106

[51] Wenjing Hong H B, Yuxi Xu, Zhiyi Yao, Zhongze Gu, and Gaoquan Shi 2010 Preparation of Gold Nanoparticle/Graphene Composites with Controlled Weight Contents and Their Application in Biosensors *The Journal of Physical Chemistry C* **114** 1822–6

[52] Sun C L, Lee H H, Yang J M and Wu C C 2011 The simultaneous electrochemical detection of ascorbic acid, dopamine, and uric acid using graphene/size-selected Pt nanocomposites *Biosensors and Bioelectronics* **26** 3450-5

[53] Xu T-Q, Zhang Q-L, Zheng J-N, Lv Z-Y, Wei J, Wang A-J and Feng J-J 2014 Simultaneous determination of dopamine and uric acid in the presence of ascorbic acid using Pt nanoparticles supported on reduced graphene oxide *Electrochimica Acta* **115** 109-15

[54] Chen L X, Zheng J N, Wang A J, Wu L J, Chen J R and Feng J J 2015 Facile synthesis of porous bimetallic alloyed PdAg nanoflowers supported on reduced graphene oxide for simultaneous detection of ascorbic acid, dopamine, and uric acid *Analyst* **140** 3183-92

[55] Liu Y, She P, Gong J, Wu W, Xu S, Li J, Zhao K and Deng A 2015 A novel sensor based on electrodeposited Au–Pt bimetallic nano-clusters decorated on graphene oxide (GO)–electrochemically reduced GO for sensitive detection of dopamine and uric acid *Sensors and Actuators B: Chemical* **221** 1542-53

[56] Tian L, Zhang B, Sun D, Chen R, Wang B and Li T 2014 A thin poly(acridine orange) film containing reduced graphene oxide for voltammetric simultaneous sensing of ascorbic acid and uric acid *Microchimica Acta* **181** 589-95